

# Natural Giesekus Fluids: Shear and Extensional Behavior of Food Gum Solutions in the Semidilute Regime

**Maria D. Torres**

Dept. of Chemical Engineering and Biotechnology, New Museums Site, University of Cambridge, Pembroke St, Cambridge, CB2 3RA, U.K.

Dept. of Chemical Engineering, University of Santiago de Compostela, Lope Gómez de Marzoa St, Santiago de Compostela, E-15782, Spain

**Bart Hallmark and D. Ian Wilson**

Dept. of Chemical Engineering and Biotechnology, New Museums Site, University of Cambridge, Pembroke St, Cambridge, CB2 3RA, U.K.

**Loic Hilliou**

Dept. of Polymer Engineering, University of Minho, Campus de Azurém, 4800-058, Guimarães, Portugal

DOI 10.1002/aic.14611

Published online September 16, 2014 in Wiley Online Library (wileyonlinelibrary.com)

*The shear and extensional behavior of two aqueous gum solutions, namely (1) 1–20 g/L guar gum (Torres et al., Food Hydrocolloids. 2014;40:85–95) and (2)  $\kappa$ /i-hybrid carrageenan solutions (5–20 g/L), are shown to exhibit Giesekus-fluid behavior when in the semidilute regime. In this regime, a common set of Giesekus fluid parameters described both shear and extensional behavior. A new analytical result describing the extension of a Giesekus fluid in the filament stretching geometry is presented. This also gave reasonable predictions of the Trouton ratio. Higher concentration guar solutions, in the entangled regime, yielded different Giesekus fluid parameters for extension to those for simple shear. The extensional data for all concentrations of both gums collapsed to a common functional form, similar to that reported for cake batters (Chesterton et al., J Food Eng. 2011;105(2):332–342); the limits of the new filament thinning expression provide insight into this behavior. © 2014 American Institute of Chemical Engineers AICHE J, 60: 3902–3915, 2014*

**Keywords:** concentration regimes, extensional, rheology, guar gum, Giesekus fluid,  $\kappa$ /i-hybrid carrageenan gum, shear rheology, Trouton ratio

## Introduction

Many liquid-based foods exhibit complex rheological behavior as a result of their multiphase nature; examples include emulsions (liquid–liquid), dense suspensions (solid–liquid), polymer solutions, bubbly liquids, and foams (both gas–liquid). The presence of a long-chain polymer or units of dispersed phase gives rise to a wide range of microstructures and deformation behaviors<sup>1</sup> that are desired in the product. The use of such materials is increasing, both in the design and formulation of new products and in supporting the replacement of traditional components such as fat and sugars in existing formulations.

Rheological testing is regularly used to establish and quantify the deformation behavior of food materials for materials characterization and quality control purposes. It is also required for process engineering studies of food systems, where rheological measurements are allied with computational fluid dynamics (CFD) simulations of equipment in

the design of new equipment and/or to confirm whether a new formulation can be processed on an existing multiproduct line. Identification of the appropriate constitutive equation, and its associated parameters, is a critical step in this process. Food processing devices, such as filling nozzles and mixers, impose a mixture of linear and extensional shear on the material<sup>2</sup> and it is important that the constitutive equation used in the CFD calculations represents both modes of deformation properly.

Whereas devices for measuring shear viscosity have been available for a long time, commercial instruments for measuring extensional viscosities accurately and independently of shear contributions are relatively new. Extensional rheometers, such as the CaBER, the FiSER, and the Cambridge Tri-master monitor the necking of extensionally strained fluid filaments as a function of time, which allows rheological parameters to be calculated.<sup>3</sup> In the absence of direct measurements, CFD calculations have had to make assumptions about the relationship between extensional and shear flow behavior, such as the magnitude of the Trouton ratio,  $Tr$ , which is the ratio of the extensional and shear viscosities at a given shear rate.<sup>4</sup> For a Newtonian fluid in uniaxial extension,  $Tr = 3$ .<sup>4</sup> The value of  $Tr$  is rarely known *a priori* for

Correspondence concerning this article should be addressed to B. Hallmark at bh206@cam.ac.uk.

complex foods as these are usually non-Newtonian and the microstructural features that give rise to non-Newtonian behavior will give rise to different dependencies on shear rate.<sup>1</sup> It is, therefore, important to establish whether there exist any cases of non-Newtonian behavior which fit a non-Newtonian constitutive equation for both linear and extensional shear behavior, so that measurements of one deformation mode can be used to predict the other with reasonable confidence, thereby reducing the amount of rheological testing.

This article demonstrates that the Giesekus constitutive equation,<sup>5</sup> which was originally developed to describe the shear behavior of polymer solutions, gives a very good description of the shear and extensional rheology of aqueous guar gum and  $\kappa/\iota$ -hybrid carrageenan gum solutions. One of the attractive features of the Giesekus equation is that it is available as standard in many commercial CFD software packages.

Guar gum is a galactomannan and one of the most cost effective natural neutral hydrocolloids due to its ready availability and ease of manufacture by extraction from *Cyamopsis tetragonoloba* seeds. This long-chain polysaccharide biopolymer is highly polydisperse, has a semi flexible random coil conformation composed of a linear mannan backbone bearing side chains of a single galactose unit, and contains a mannose to galactose ratio of approximately 1.6–1.8:1. Guar gum is widely used in food and other applications as a thickener and rheology modifier. Aqueous solutions are shear thinning, and several studies<sup>6–9</sup> have demonstrated that its nonlinear shear rheology can be described very well by the Cross model.<sup>10</sup> The Cross model, however, is a generalized Newtonian model and hence does not provide an *a priori* estimate of extensional behavior.

Carrageenans are natural linear polysaccharides extracted from red seaweeds (*Gigartinales*, *Rhodophyta*) and are extensively used as thickeners, gelling, texturing, suspending, or stabilizing agents.<sup>11</sup> Most carrageenophyte seaweeds produce  $\kappa/\iota$ -hybrid carrageenans, and alternative algal resources for carrageenan production are needed to cope with the steadily increasing demand for food texturing agents.<sup>11</sup> They are natural polyelectrolyte copolymers comprising blocks of  $\kappa$  or  $\iota$ -carrageenan disaccharide units randomly distributed along the chain, together with minor amounts of nongelling disaccharide units (biological precursors). The relative amount of  $\kappa$  or  $\iota$ -depends on the plant biology and the biopolymer extraction procedure. The chemical structure of  $\kappa/\iota$ -hybrid carrageenans has a direct impact on its gel properties as reported recently.<sup>12–14</sup>

The extensional rheology of guar gum solutions has been studied widely,<sup>8,15,16</sup> whereas there are no studies to date of aqueous  $\kappa/\iota$ -hybrid carrageenan solutions. Bourbon et al. used a CaBER device to study a narrow range of guar gum concentrations (0.39–0.97 g/L) and compared their results with finitely extensible nonlinear elastic (FENE) constitutive models. We have recently presented measurements<sup>1</sup> of the extensional rheology of guar gum solutions obtained using the Cambridge Trimaster filament stretching device<sup>17</sup> over a wider range of concentrations (1–20 g/L), crossing the transition from the semidilute to the entangled regime. It will be shown that the Giesekus equation provides a good description of both linear and extensional shear behavior of both these datasets and new sets obtained for  $\kappa/\iota$ -hybrid carrageenan solutions.

The Giesekus model has been widely used to describe the shear response of solutions of synthetic polymers.<sup>18,19</sup> It has received little attention in the literature on food polymer solutions, even though it is able to account for both the low and high shear rate plateau viscosities and the shear-thinning behavior reported for many viscous food liquids. It has also been used to describe the extensional viscosity of synthetic polymers.<sup>3,20,21</sup> Anna and McKinley<sup>3</sup> fitted a multimode Giesekus model to data obtained from filament stretching of Boger fluids consisting of high molecular weight polystyrene dissolved in styrene oil: this required the solution of a set of coupled ordinary differential equations. This article presents the derivation of a simple analytical expression that predicts the time-dependent viscoelastic filament thinning of a single-mode Giesekus fluid. This is found to give a good description of the experimental data obtained for the guar gum and  $\kappa/\iota$ -hybrid carrageenan gum solutions. We are not aware of this result being presented previously elsewhere. It allows the extensional behavior to be compared with that expected from (linear) shear measurements. The ability to predict extensional behavior from shear flow measurements is tested and shown to depend on whether the solution is semidilute and unentangled or whether the solution exists in the entangled regime.

## Experimental

### Sample preparation

Commercial guar gum was supplied by Sigma-Aldrich (batch no. 041M0058V, India). The  $\kappa/\iota$ -hybrid carrageenan gum was extracted from *M. stellatus* seaweed using the method described by Hilliou and coworkers.<sup>13</sup> Aqueous solutions of guar gum (reported by Torres and coworkers<sup>1</sup>) and  $\kappa/\iota$ -hybrid carrageenan gum over a wide range of concentrations (1–20 g/L) were prepared following procedures established in the literature.<sup>7,12</sup> The guar gum was dispersed in tap water by stirring at 1400 rpm overnight on a magnetic hotplate stirrer (VMS-C4 Advanced, VWR, UK) at room temperature, between 19°C and 21°C, to ensure complete hydration of the gums. The aqueous  $\kappa/\iota$ -hybrid carrageenan gum solutions were prepared by dissolving the gum in NaCl 0.1 M solutions, to fix the ionic strength. Some air was incorporated into the solution during stirring and deaerated samples of the continuous phase were obtained by centrifugation at 2250 rpm (500 g) for 5 min. All samples were, at minimum, duplicated.

### Rheology measurements

Steady shear measurements were performed on a Bohlin CVO120HR controlled-stress rheometer (Malvern Instruments, Malvern, UK) using sand-blasted parallel plates (25-mm diameter and 1-mm gap) to prevent wall slippage. The normal force generated by the flow between plates was also measured. Measurements of axial thrust were used to estimate the normal stress difference,  $N_1 - N_2$ <sup>4</sup>; calibration of this device indicated that reliable axial thrust data could be acquired for thrusts greater than  $9.8 \times 10^{-3}$  N. Samples were loaded carefully to ensure minimal structural damage, and held at rest for 5 min before testing to allow stress relaxation and temperature equilibration. A thin film of a Newtonian silicone oil (viscosity 1 Pa s) was applied to the exposed sample edges to prevent evaporation. All

measurements were made under isothermal conditions (20°C) and, at minimum, duplicated.

Extensional measurements were investigated using the Cambridge Trimaster, a high-speed filament stretch and break-up device.<sup>17</sup> The apparatus consists of two cylindrical 1.2 mm diameter stainless steel stubs which are moved vertically apart at speed with high spatial precision. Measurements reported here featured an initial gap spacing of 0.6 mm, final gap spacing of 1.5 mm, and piston separation speed of 75 mm s<sup>-1</sup>. The initial filament diameter,  $D_1$ , was measured once the stainless steel stubs had reached their final position; this parameter was strongly dependent on the fluid properties and was often slightly different for each experiment. The filament stretching and thinning profiles were monitored using a high-speed camera (Photron Fastcam 1024 PCI) which allows the diameter of the filament mid-point to be measured to within 1 μm at a rate of 6000 frames per second. The device did not feature a force transducer so separating forces were not recorded. All experiments were performed at least in duplicate in an air-conditioned room at 20°C. Error bars corresponding to experiment variation of repeated steady shear and extensional tests are plotted where the measurement uncertainty was greater than the symbol size. Further information about the protocols used can be found in a previous publication.<sup>1</sup>

## Theory

### Giesekus model for shear behavior

The total stress in a fluid,  $\sigma$ , is written as

$$\sigma = -p\mathbf{I} + \tau \quad (1)$$

where  $p$  is the hydrostatic pressure and  $\mathbf{I}$  the identity tensor. In the Giesekus constitutive equation,<sup>5,22</sup> the shear stress,  $\tau$ , is modeled as

$$\frac{\tau}{\lambda} + \frac{\partial \tau}{\partial t} + \mathbf{v} \cdot \nabla \tau - \left( (\nabla \mathbf{v})^T \tau + \tau (\nabla \mathbf{v}) \right) = \frac{\eta_0}{\lambda} \dot{\gamma} - \frac{a}{\eta_0} \tau \cdot \tau \quad (2)$$

where  $\mathbf{v}$  is the velocity vector,  $\eta_0$  is the zero shear (Newtonian) viscosity,  $t$  is time,  $\lambda$  is the characteristic relaxation time, and  $a$  is the mobility parameter; the mobility parameter describes the anisotropy of hydrodynamic drag and Brownian motion on the polymer molecule.<sup>23</sup> The rate-of-strain-tensor,  $\dot{\gamma}$ , is

$$\dot{\gamma} = (\nabla \mathbf{v}) + (\nabla \mathbf{v})^T \quad (3)$$

Expressions that describe the shear rate dependence of the shear viscosity as a function of shear rate for a single-mode Giesekus fluid have been presented in the literature.<sup>5</sup> These expressions have been successfully applied to describe the flow curve of aqueous solutions of rod-like micelles for the surfactant system cetyltrimethylammonium,<sup>20</sup> and are used here to describe the steady, one dimensional, shear response of guar gum and  $\kappa$ /ι-hybrid carrageenan gum solutions of varying concentrations. In summary

$$\eta(\dot{\gamma}) = \frac{\eta_0(1-n_2)}{1+(1-2a)n_2} \quad (4)$$

Here, the dimensionless terms  $n_2$  and  $\Lambda$  are given by

$$n_2 = \frac{1-\Lambda}{1+(1-2a)\Lambda} \quad (5)$$

$$\Lambda = \sqrt{\frac{\sqrt{1+16a(1-a)\lambda^2\dot{\gamma}^2}-1}{8a(1-a)\lambda^2\dot{\gamma}^2}} \quad (6)$$

For steady shear at steady shear rate, Eq. 2 implies that first normal stress difference,  $N_1$ , is of the form<sup>24,25</sup>

$$N_1 = 2\lambda\eta_0 \frac{n_2(1-n_2)}{\lambda^2 a(1-n_2)} \quad (7)$$

Over some concentration ranges, the second normal stress difference,  $N_2$ , has been observed to be  $N_2 \sim -N_1/10$ .<sup>26</sup> For this work, however, the analytical form of the second normal stress difference for a Giesekus fluid was used<sup>25</sup>

$$N_2 = \frac{-aN_1}{2} \frac{(1-n_2)}{(1-n_2)} \quad (8)$$

Equations 7 and 8 were then used to estimate the magnitude of the stress difference,  $N_1 - N_2$ , measured in the steady shear experiments.

### Derivation of a simple expression for the extensional behavior of a Giesekus fluid

The derivation of the extensional thinning of a filament of cylindrical thread of a Giesekus fluid follows similar lines to that of Entov and Hinch,<sup>27</sup> in their analysis of the filament breakup of dilute polymer solutions using a FENE model.<sup>28</sup> Other authors, notably the McKinley group at MIT, have derived simple expressions that describe viscoelastic filament breakup using the FENE-P model<sup>3</sup> along with models involving coupled ordinary differential equations that describe the filament breakup of Giesekus fluids.<sup>29</sup> This section presents the derivation of a simple expression that predicts time-dependent viscoelastic filament thinning of a single-mode Giesekus fluid.

The first simplification made is to assume that extensional deformations only occur in the axial and radial directions within the liquid filament, and that the divergence of the extra stress tensor is zero. This allows Eq. 2 to be simplified to a pair of ordinary differential equations, which are a function of the axial and radial components of the stress within the filament, viz

$$\frac{\tau_{zz}}{\lambda} + \frac{\partial \tau_{zz}}{\partial t} - \tau_{zz}\dot{\gamma}_{zz} = \frac{\eta_0}{\lambda} \dot{\gamma}_{zz} - \frac{a}{\eta_0} \tau_{zz}^2 \quad (9)$$

$$\frac{\tau_{rr}}{\lambda} + \frac{\partial \tau_{rr}}{\partial t} - \tau_{rr}\dot{\gamma}_{rr} = \frac{\eta_0}{\lambda} \dot{\gamma}_{rr} - \frac{a}{\eta_0} \tau_{rr}^2 \quad (10)$$

The boundary conditions on the liquid filament assume that any end effects, where the liquid filament may contact a surface, are negligible resulting in zero axial stress. This assumption is commonly used when deriving expressions for extensional thinning<sup>30</sup> but strictly speaking requires experimental validation. Alternative assumptions can include an exponential increase in normal stress for viscoelastic fluids.<sup>31</sup> Furthermore, it is assumed that surface tension,  $\alpha$ , alone is responsible for the radial stress that causes the filament to thin, with the radial stress being assumed to be equal to the Laplace pressure. These boundary conditions can be derived from Eq. 1 and give

$$\sigma_{zz} = 0 = -p + \tau_{zz} \quad (11)$$

$$\sigma_{rr} = -p + \tau_{rr} = -\frac{2\alpha}{D} \quad (12)$$

Equation 11 allows the unknown hydrostatic pressure,  $p$ , to be calculated, which can then be substituted into Eq. 12; this leads to an expression that relates the radial and axial

components of the stress to the surface tension and to the filament diameter. It is now assumed that the axial extensional stress is the dominant stress in the problem giving the following relationship between this stress, the surface tension and filament diameter,  $D$ .

$$\tau_{zz} \approx \frac{2\alpha}{D} \quad (13)$$

To calculate the variation of the filament diameter as a function of time, the strain rate in the radial direction can be related to the change in velocity in the radial direction velocity, that is

$$\dot{\gamma}_{rr} = 2 \frac{\partial v_r}{\partial r} \quad (14)$$

This, in turn, can then be related to the filament diameter, giving

$$\dot{\gamma}_{rr} = 2 \frac{\partial}{\partial r} \left( \frac{\partial r}{\partial t} \right) = \frac{4\partial}{\partial D} \left( \frac{1}{2} \frac{\partial D}{\partial t} \right) = 2 \frac{\partial^2 D}{\partial D \partial t} \quad (15)$$

Integration of Eq. 15 with respect to the filament diameter yields a simple ordinary differential equation in terms of radial direction shear rate

$$\frac{dD}{dt} = -\frac{\dot{\gamma}_{zz}}{4} D \quad (16)$$

The radial and axial components of the strain rate can then be related by remembering that the deformation is a uniaxial extension. The expressions for axial extension rate, Eq. 16, and approximate axial tensile stress, Eq. 13, can now be substituted into the axial component of the Giesekus expression, which was shown in Eq. 9. The resulting expression is

$$\frac{2\alpha}{D\lambda} + 2\alpha \frac{d}{dt} \left( \frac{1}{D} \right) + \frac{8\alpha}{D^2} \frac{dD}{dt} = \frac{-4\eta_0}{D\lambda} \frac{dD}{dt} - \frac{4\alpha\lambda^2}{\eta_0 D^2} \quad (17)$$

Some manipulation and reorganization of the terms in Eq. 17 result in a single, nonlinear, ordinary differential equation that relates the rate of change of filament diameter to the physical properties of the fluid

$$\frac{dD}{dt} = \frac{-\alpha}{\eta_0} \left( \frac{\eta_0 D + 2a\lambda\alpha}{2\eta_0 D + 3\alpha\lambda} \right) \quad (18)$$

Integration of Eq. 18, subject to the initial condition that at  $t = 0$  the initial filament diameter is  $D_1$ , yields

$$\frac{\alpha\lambda(3-4a)}{\eta_0} \ln \left( \frac{\eta_0 D + 2a\lambda\alpha}{\eta_0 D_1 + 2a\lambda\alpha} \right) + 2(D - D_1) = \frac{-\alpha t}{\eta_0} \quad (19)$$

An analogous derivation for an upper convected Maxwell (UCM) fluid<sup>32</sup> makes the assumption that viscous stresses are negligibly small when compared to elastic stresses. For the condition that both  $a = 0$  and  $\eta_0 = 0$ , Eq. 19 simplifies to the expected UCM result for extensional filament thinning where  $D/D_1 = \exp(-t/3\lambda)$ . Equation 19 relates the filament diameter implicitly to time, making it more straightforward to calculate the variation in time as a function of a given filament diameter, rather than *vice versa*. Equation 19 can also be expressed in nondimensional form as

$$(4a-3) \ln \left( \frac{\left( \frac{D}{D_1} \right) + \frac{2a\lambda\alpha}{D_1\eta_0}}{1 + \frac{2a\lambda\alpha}{D_1\eta_0}} \right) - \frac{2\eta_0 D_1}{\alpha\lambda} \left( \frac{D}{D_1} - 1 \right) = \frac{t}{\lambda} \quad (20)$$

Equation 20 highlights that there are two contributions to the characteristic timescale for the thinning of the liquid

thread. The first term on the left-hand side (LHS) contains the Giesekus mobility parameter, which relates to the anisotropic relaxation of the polymer chains. The second term, which would also arise from the UCM constitutive equation, contains terms that relate to the longest relaxation time, zero shear rate viscosity and surface tension alone.

In the absence of direct measurements of extensional force (as in the case of the Trimaster device used to collect the extensional data presented here), it is possible to estimate the extensional viscosity,  $\eta_E$ , of a fluid undergoing a uniaxial extension using<sup>17</sup>

$$\eta_E = (2X-1) \frac{-\alpha}{dD/dt} \quad (21)$$

In this expression,  $X$  is a coefficient that accounts for the deviation of the filament shape from a uniform cylinder due to inertia and gravity; in other studies this has been assumed to be roughly 0.7.<sup>17,33</sup> Combining Eq. 18 with Eq. 21 yields the following estimate of the extensional viscosity of a Giesekus fluid

$$\eta_E = \eta_0 (2X-1) \frac{3+2\eta_0 D/\alpha\lambda}{2a+\eta_0 D/\alpha\lambda} \quad (22)$$

Equation 22 allows the extensional viscosity to be estimated relatively simply for a Giesekus fluid. Other methods<sup>34</sup> of estimating the extensional viscosity for FENE fluids are described in the literature; these involve interpolation between the asymptotic and perturbation solutions that, respectively, describe the limiting cases of extensional viscosity a large and small extension rates.

## Statistical analysis

The parameters of the models considered were determined from the experimental data with a one-factor analysis of variance (ANOVA) using PASW Statistics (v.18, IBMSPSS Statistics, NY). When the ANOVA indicated differences among means, a Scheffé test was performed to differentiate means with 95% confidence ( $P < 0.05$ ).

## Results and Discussion

### Concentration regimes

Both the guar gum and carrageenan solutions were found to be shear thinning and highly viscoelastic, with each property being strongly dependent on concentration. The effect of concentration on the guar gum solutions was investigated in our previous paper<sup>1</sup> and the results are summarized here alongside new results for the  $\kappa/\iota$ -hybrid carrageenan solutions.

The dynamic response of the guar gum solutions to oscillatory shear testing indicated a transition from being predominantly viscous, at concentrations below approximately 5 g/L to exhibiting a significant elastic response at higher concentrations. This transition was not observed in the  $\kappa/\iota$ -hybrid carrageenan gum solutions, which indicated predominantly viscous behavior over the frequency range investigated (data not reported) for all concentrations tested. This suggested that the carrageenan solutions were in the semidilute regime, while the higher concentrations of guar gum were subjected to significant entanglements.

Another observation suggesting that the threshold of the entangled regime for the guar gum solutions lay near 10 g/L was that the measured surface tension deviated from the



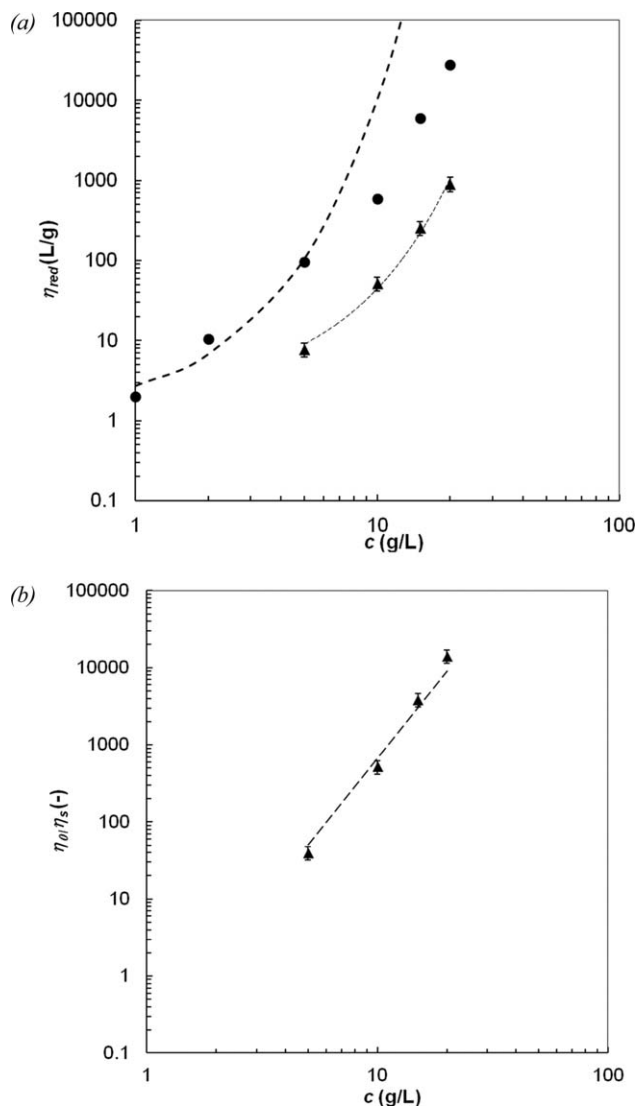


**Figure 1. Effect of guar gum (circles) and  $\kappa/\iota$ -hybrid carrageenan gum (triangles) concentration on reduced viscosity.**

Data points for guar gum are computed from experimental  $\eta_0$  data from Torres and coworkers.<sup>1</sup> Dashed lines in (a) are fits of Eq. 23 to the first three data points for guar gum solutions and to the whole set of data for  $\kappa/\iota$ -hybrid carrageenan gum solutions. Dashed lines in (b) denote power law regression.

Szyszkowski equation<sup>35</sup> at 10 g/L, indicating that the solution was exhibiting behavior analogous to that associated with critical aggregation concentration.<sup>36</sup> This is consistent with other reported studies of guar gum solutions.<sup>37,38</sup> In contrast, the concentration dependence of surface tension of  $\kappa/\iota$ -hybrid carrageenan gum solutions was satisfactorily fitted to the Szyszkowski equation<sup>35</sup> over the whole concentration range studied (see Appendix, Figure A1).

In the semidilute coil overlap region, the reduced viscosity,  $\eta_{red}$ , is expected to follow the Martin equation,<sup>39</sup> viz

$$\frac{\eta_0 - \eta_s}{c\eta_s} = \eta_{red} = [\eta] \exp(k[\eta]c) \quad (23)$$

where  $\eta_s$  is the solvent viscosity,  $c$  the solution mass concentration,  $[\eta]$  the intrinsic viscosity and  $k$  the Huggins parameter. In this region, the coil overlap parameter,  $c[\eta]$ , is

expected to lie between  $1 < c[\eta] < 10$ . The zero shear rate viscosity values were used to estimate  $\eta_{red}$  and are plotted against  $c$  in Figure 1a. The guar gum data fit Eq. 23 reasonably for  $c \leq 5$  g/L but deviate strongly from the trend at higher concentrations. Linear regression yielded  $[\eta] = 1.09 \pm 0.02$  L/g and  $k = 0.84 \pm 0.07$ , which compare favorably with the values for similar gums,<sup>40</sup> namely  $[\eta] = 1.06$  L/g, and  $k = 1.07$  at 24°C and 0.73 at 45°C. Other studies of guar gum and similar materials<sup>4,7,8</sup> have reported similar behavior. The  $\kappa/\iota$ -hybrid carrageenan gum data showed a good fit to Eq. 23 over the whole concentration range studied, giving  $[\eta] = 1.05 \pm 0.01$  L/g and  $k = 0.34 \pm 0.03$ . The  $[\eta]$  values are consistent with those previously reported for  $\kappa/\iota$ -hybrid carrageenan gum solutions.<sup>41</sup> Values of  $k < 0.5$  indicate systems where the solvent-polymer interactions are favored over polymer-polymer interactions.<sup>39,40</sup> The polyelectrolyte nature of the  $\kappa/\iota$ -hybrid carrageenan gum is mirrored in Figure 1b. The double logarithmic plot confirms the expected power law behavior for polyelectrolytes polymers approaching the theoretical one,

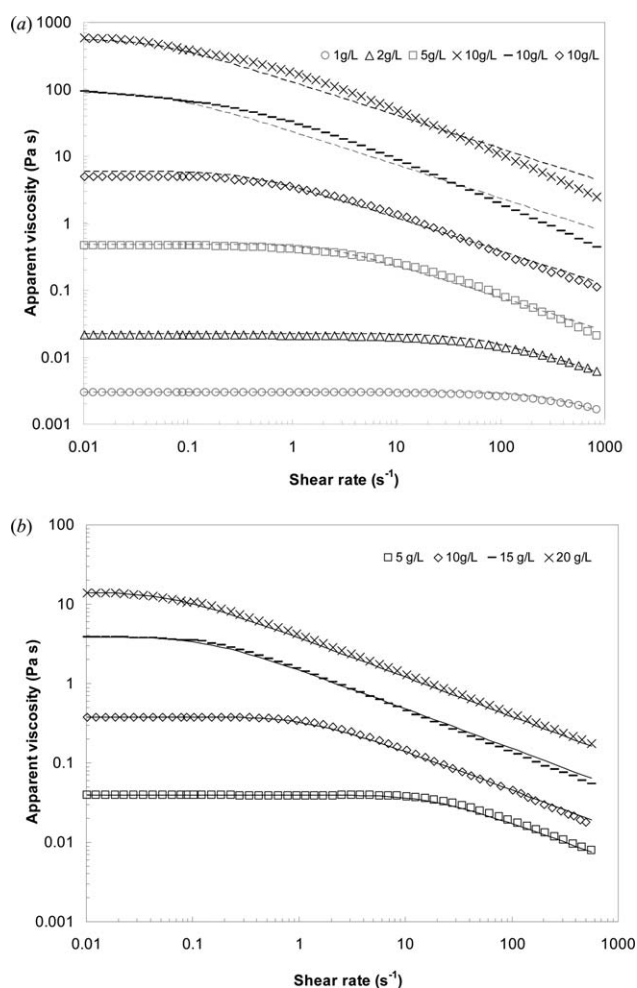


**Figure 2. Comparison of the measured apparent viscosity of (a) guar gum solutions (reproduced from Torres and coworkers<sup>1</sup>) and (b)  $\kappa/\iota$ -hybrid carrageenan gum solutions with the Giesekus model, Eq. 4.**

Concentration: 1 g/L (open gray circles); 2 g/L (open black triangles); 5 g/L (open gray squares); 10 g/L (open black diamonds); 15 g/L (dashes); and 20 g/L (crosses). Dashed loci indicate model fit, parameters in Table 1.

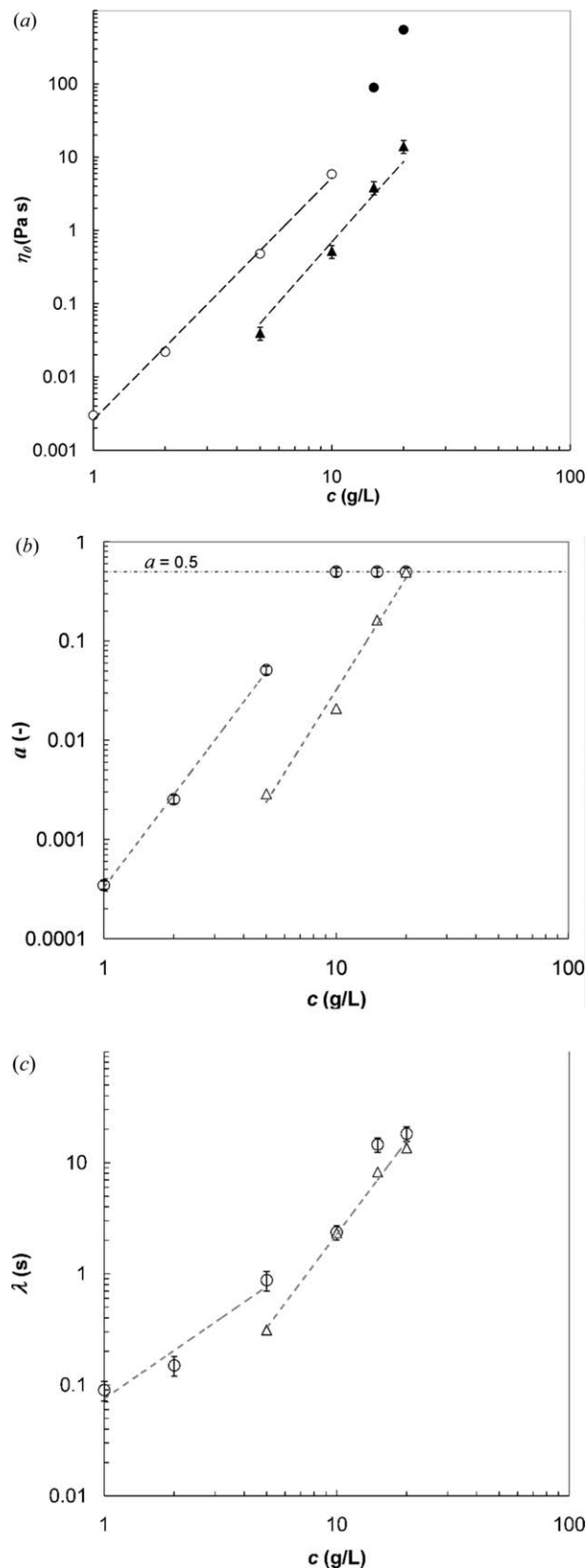


**Figure 3.** Effect of concentration on Giesekus model parameters.

(a)  $\eta_0$ ; (b)  $a$  and (c)  $\lambda$  for guar gum and  $\kappa/\iota$ -hybrid carrageenan gum. Dashed loci shows the power law trend line, Eq. 24, fitted to the data for solutions in the semidilute regime, parameters given in Table 1. Symbols: circles—guar gum solutions, triangles— $\kappa/\iota$ -hybrid carrageenan gum solutions.

$\eta_0/\eta_s \sim k' c^{15/4}$  for semi dilute-entangled regime of polyelectrolyte solutions,<sup>42</sup> with  $k'$  values of 0.12.

### Shear-thinning behavior

The shear flow data for both gums gave a good fit to the Cross model<sup>1</sup> for the guar gum data, carrageenan results provided in the Appendix, Figure A2, but this model does not provide insight into extensional behavior. Figure 2a shows that the Giesekus model (Eq. 4) gives a good description ( $R^2 > 0.988$ ) of the shear flow data for guar gum solutions in the semidilute regime ( $c = 1\text{--}5$  g/L). There is an increasingly poorer fit in the entangled regime as the concentration increases ( $\geq 10$  g/L). In contrast, Figure 2b shows that the  $\kappa/\iota$ -hybrid carrageenan gum solutions exhibited Giesekus-fluid behavior over the whole concentration range studied.

Equation 4 has three adjustable parameters: the zero shear rate viscosity, the Giesekus mobility parameter and the relaxation time;  $\eta_0$  was taken from the experimental data at the

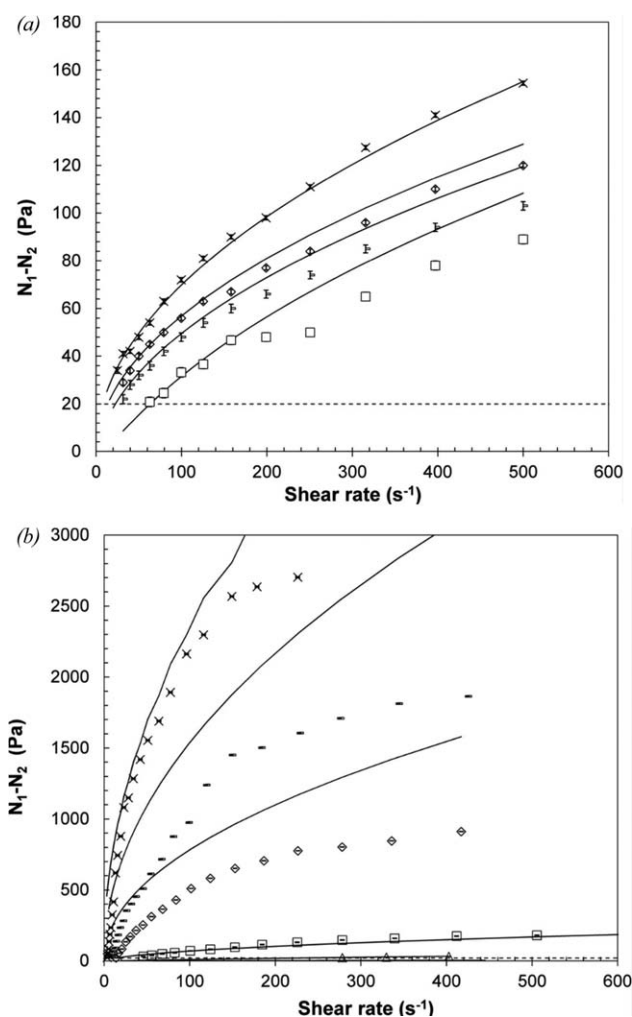


**Figure 4.** Normal stress differences ( $N_1 - N_2$ ) measured for aqueous (a)  $\kappa/\iota$ -hybrid carrageenan gum and (b) guar gum solutions prepared at different polymer concentration.

Lines show the difference between Eqs. 7 and 8 fitted to the data for studied solutions. Concentration: 2 g/L (open black triangles); 5 g/L (open gray squares); 10 g/L (open black diamonds); 15 g/L (dashes); and 20 g/L (crosses). The dashed horizontal line corresponds to the noise floor of the normal force transducer.

**Table 1. Values of Power Law Factor,  $K^*$ , and Power Law Exponent,  $n$ , Required to Estimate the Relationship Between Material Properties,  $f(c)$ , and Solution Concentration**

Parameter	Guar Gum		$\kappa/\iota$ -Hybrid Carrageenan Gum	
	$K^*$	$n$	$K^*$	$n$
Zero shear rate viscosity, $\eta_0$	$(2.60 \pm 0.02) \times 10^{-3}$	$3.30 \pm 0.03$	$(4.01 \pm 0.03) \times 10^{-5}$	$3.75 \pm 0.02$
Mobility parameter, $a$	$(3.20 \pm 0.01) \times 10^{-4}$	$3.17 \pm 0.05$	$(9.05 \pm 0.02) \times 10^{-6}$	$3.60 \pm 0.03$
Relaxation time, $\lambda$	$(7.37 \pm 0.04) \times 10^{-2}$	$1.49 \pm 0.10$	$(3.7 \pm 0.03) \times 10^{-3}$	$2.79 \pm 0.08$

Units of  $K^*$  are [parameter] (g/L)<sup>-n</sup>

lowest shear rate studied, 0.01 s<sup>-1</sup>. The remaining two parameters,  $a$  and  $\lambda$ , were fitted to the experimental data by a least squares algorithm and the results are presented in Figure 3. Several workers<sup>43,44</sup> have reported that although the theoretical range of the mobility parameter is  $0 < a < 1$ , physically realistic solutions are only obtained for the range  $0 < a < 0.5$ . An upper limit of 0.5 was hence used here.

The fit in Figure 2a obtained for higher concentrations for guar gum solutions is arguably less good than at lower concentrations, due to the limitation of having a single relaxation time. Figure 2a also shows a marked increase in apparent viscosity with concentration. The highest concentration in these tests, 20 g/L, corresponds to a polymer volume fraction of 0.055 and Figure 2a shows an increase of six orders of magnitude in  $\eta_0$  for a 20 $\times$  increase in guar gum concentration. A similar trend is seen with the  $\kappa/\iota$ -hybrid carrageenan, Figure 2b, albeit with a smaller increase (four orders of magnitude) over the concentration range.

Figure 3 shows that all three Giesekus parameters exhibited a strong dependency on concentration in the semidilute regime. The plots show that these data could be described reasonably well by power law relationships of the form

$$f(c) = K^* c^n \quad (24)$$

with the values of the prefactor,  $K^*$ , and power law index,  $n$ , obtained by regression presented in Table 1. Above a critical concentration of 10 g/L guar gum solutions did not fit these trends, with  $\eta_0$  and  $\lambda$  exceeding the values obtained by extrapolation, and  $a$  reaching the upper limit of 0.5.

In the semidilute region  $\eta_0$  and  $a$  exhibit similar sensitivity to  $c$ , with  $n \sim 3$  for guar gum solutions and  $n \sim 4$  for  $\kappa/\iota$ -hybrid carrageenan gum solutions, while the relaxation time is less sensitive to  $c$ , with  $n \sim 2$  and 3, respectively. These values can be compared with those expected

from scaling theories, but this was not pursued here as only one sample of each gum was studied here. More detailed studies with gums of different molecular weight should follow. These results suggest that the Giesekus parameters in the semidilute regime can be estimated for engineering purposes from knowledge of the solution concentration alone.

The normal stress difference data,  $N_1 - N_2$ , presented in Figure 4 indicate that  $\kappa/\iota$ -hybrid carrageenan gum solutions generate smaller elastic responses than those featured in guar gum solutions. The aqueous guar gum solutions show appreciable elastic responses at high shear rates.  $N_1 - N_2$  for guar gum solutions at 2 g/L was practically negligible, in that the measured thrust lay within the noise floor for the rheometer whereas for  $c = 20$  g/L  $N_1 - N_2$  increased rapidly at shear rates above 1 s<sup>-1</sup>. The shear rate at which  $N_1 - N_2$  increased noticeably was smaller at higher concentrations. Furthermore, the shear rate at which  $N_1 - N_2$  increased corresponds to the onset of noticeable shear thinning in Figure 2. The  $N_1 - N_2$  values of  $\kappa/\iota$ -hybrid carrageenan gum solutions approached a common value at high shear rates.

Figure 4 also shows that the normal stress differences predicted by Eqs. 7 and 8, gives very good agreement for the guar gum solutions in the semidilute regime and all the  $\kappa/\iota$ -hybrid carrageenan gum solutions tested. It should be noted that the lines in Figure 4 are computed using the parameters obtained from fitting the Giesekus model (Eq. 4) to the shear stress data, not the measured normal force. The values of the model parameters  $\eta_0$ ,  $\lambda$ , and  $a$  are those given in Table 2.

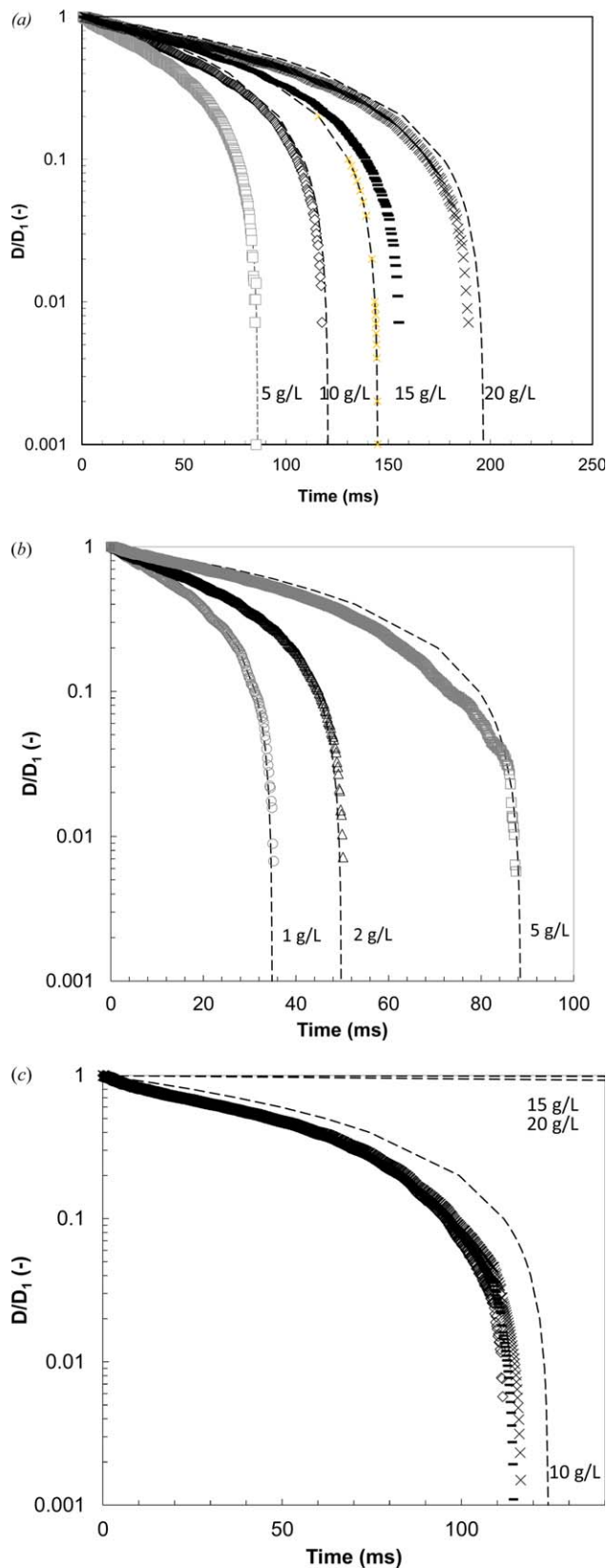
### Filament stretching behavior

Plots of filament stretching data such as those in Figure 5 exhibit features observed in other studies, namely an initially

**Table 2. Parameters Obtained by Fitting Eq. 4 to Guar Gum and  $\kappa/\iota$ -Hybrid Carrageenan Solutions Shear Data in Figure 2**

Solution Concentration $C$ (g/L)	Mobility Parameter $a$ (-)	Relaxation Time $\lambda$ (s)	Surface Tension $\alpha$ (N/m)	Zero Shear Rate Viscosity $\eta_0$ (Pa s)	Initial Filament Diameter $D_1$ ( $\mu$ m)	$R^2$ Value (-)
Guar gum						
1	$0.00035 \pm 0.00001^d$	$0.090 \pm 0.003^f$	$0.0685 \pm 0.0002^a$	$0.0029 \pm 0.0002^f$	$205 \pm 2^f$	0.993
2	$0.0026 \pm 0.0002^c$	$0.150 \pm 0.002^e$	$0.0675 \pm 0.0003^b$	$0.022 \pm 0.003^c$	$280 \pm 3^e$	0.992
5	$0.051 \pm 0.002^b$	$0.878 \pm 0.002^d$	$0.0675 \pm 0.0002^b$	$0.480 \pm 0.004^d$	$430 \pm 1^d$	0.988
10	$0.50 \pm 0.00^a$	$2.37 \pm 0.01^c$	$0.0674 \pm 0.0001^b$	$5.87 \pm 0.05^c$	$477 \pm 3^c$	0.950
15	$0.50 \pm 0.00^a$	$14.5 \pm 0.1^b$	$0.0673 \pm 0.0001^b$	$89.5 \pm 0.2^b$	$482 \pm 1^b$	0.891
20	$0.50 \pm 0.00^a$	$18.2 \pm 0.2^a$	$0.0672 \pm 0.0001^b$	$550 \pm 12^a$	$487 \pm 2^a$	0.886
$\kappa/\iota$ -hybrid carrageenan gum						
5	$0.0029 \pm 0.0004^d$	$0.312 \pm 0.003^d$	$0.0725 \pm 0.0002^a$	$0.040 \pm 0.002^d$	$316 \pm 1^b$	0.995
10	$0.021 \pm 0.002^c$	$2.33 \pm 0.05^c$	$0.0714 \pm 0.0002^b$	$0.381 \pm 0.003^c$	$319 \pm 1^{a,b}$	0.996
15	$0.18 \pm 0.01^b$	$8.24 \pm 0.04^b$	$0.0709 \pm 0.0002^c$	$3.85 \pm 0.04^b$	$321 \pm 1^a$	0.993
20	$0.495 \pm 0.00^a$	$13.55 \pm 0.06^a$	$0.0703 \pm 0.0002^d$	$14.1 \pm 0.1^a$	$324 \pm 2^a$	0.990

Data are presented as mean  $\pm$  standard deviation. Data values in a column with different superscript letters are significantly different at the  $P \leq 0.05$  level.



linear decrease in  $\ln D/D_1$  with time followed a steep reduction in  $D/D_1$  as the filament approaches rupture at time  $t_F$ .

The guar gum and  $\kappa/\iota$ -hybrid carrageenan gum data were compared with existing models for extension of single- and multimode FENE materials<sup>3,27</sup> and gave a poor fit. In contrast, the single-mode Giesekus model, Eq. 2, gives good agreement for both the guar gum solutions at lower concentrations and all the  $\kappa/\iota$ -hybrid carrageenan gum solutions tested. It should be emphasized that lines in Figure 5 are computed with Eq. 19, using the parameters obtained from fitting the Giesekus model (Eq. 4) to the data from shear experiments (see Figure 2): the values of the model parameters  $\eta_0$ ,  $\lambda$ , and  $a$  are those given in Table 1. The values of the liquid-air surface tension,  $\alpha$ , in Eq. 19 for guar gum are those previously reported,<sup>1</sup> while the values for the  $\kappa/\iota$ -hybrid carrageenan solutions were determined for this study using the same protocol (see Appendix, Figure A1).

The agreement between the experimental data and the prediction for  $\kappa/\iota$ -hybrid carrageenan gum solutions prepared at 5 g/L (Figure 5a) and for the semidilute guar gum solutions prepared at 1 g/L and 2 g/L (Figure 5b) is excellent ( $R^2 > 0.990$ ). The filament rupture time, when  $D/D_1$  approaches zero rapidly, is predicted quite well for the 5 g/L case but the evolution in  $D/D_1$  prior to this deviates noticeably from the model. These results indicate that Eq. 19 is able to describe the extensional behavior of the semidilute guar gum solutions with parameters obtained from shear flow tests. The converse is expected to follow, that shear flow behavior could be predicted using extensional tests. Extensional tests have the advantage of requiring very small volumes of liquids; however, shear flow devices are able to assess the influence of phenomena such as wall slip; this could not be predicted from extensional testing alone.

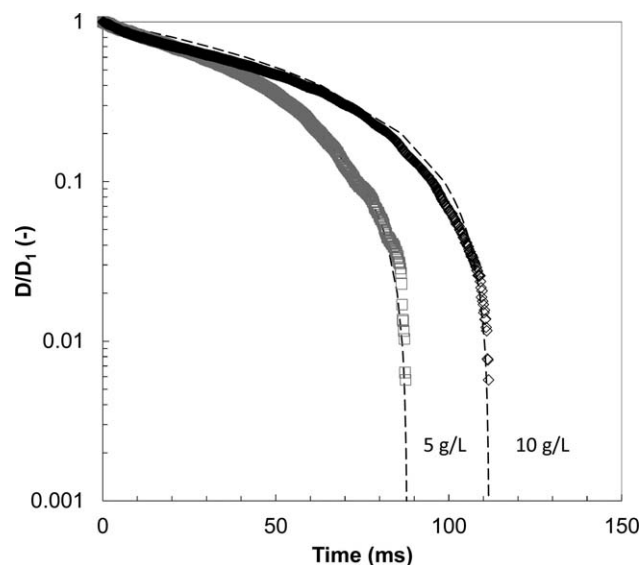


**Figure 6.** Fitting of guar gum solution filament stretching data in Figure 4c to Eq. 19 when Giesekus model parameters  $a$  and  $\lambda$  are allowed to differ from those obtained from fitting shear flow data (Figure 2a).

Dashed loci—model fit with parameters given in Table 3.



**Table 3. Parameters Obtained by Fitting Eq. 19 to Guar Gum Solution Extensional Data in Figure 6 Compared Against Those Obtained Using the Shear Data Shown in Figure 2**

Concentration $C$ (g/L)	Shear Flow (Figure 2)		Extensional Shear (Figure 6)		$R^2$ Value (-)
	$a$ (-)	$\lambda$ (s)	$a$ (-)	$\lambda$ (s)	
5	$0.051 \pm 0.002^b$	$0.878 \pm 0.002^b$	$0.032 \pm 0.005^b$	$0.029 \pm 0.001^a$	0.994
10	$0.50 \pm 0.00^a$	$2.37 \pm 0.01^a$	$0.461 \pm 0.003^a$	$0.023 \pm 0.002^a$	0.995

Data are presented as mean  $\pm$  standard deviation. Data values in a column with different superscript letters are significantly different at the  $P \leq 0.05$  level.

Figure 5c shows progressively less good agreement between the experimental data and the model predictions as guar gum concentration increases within the entangled regime. At 10 g/L, where entanglement is apparent, and there is an associated increase in the magnitude of the elastic response,<sup>1</sup> Eq. 19 does not give a good prediction of the extensional behavior when the parameters obtained from

Eq. 4 are used. The fit is even poorer with higher concentrations.

The derivation of Eq. 19 involves the assumption that the axial stress dominates over the radial stress; guar gum solutions that have a significant elastic response will also have significant first normal stress differences,<sup>1</sup> possibly invalidating this assumption. This may be the cause of the failure of Eq. 19 to fit the data at high concentrations. It may also be the case, however, that the constitutive model needs to be revised to capture the phenomena associated with the extension of the guar gum solutions, such as using a multimode formulation. The approach taken here was to allow the mobility parameter,  $a$ , and relaxation time,  $\lambda$ , to differ from the values obtained from the shear flow data in Figure 2.  $D_1$ ,  $\eta_0$ ,  $\eta_\infty$ , and  $\alpha$  are not altered. Figure 6 shows that Eq. 19 gives a very good fit ( $R^2 > 0.992$ ) to the data at 5 and 10 g/L if the mobility parameter and relaxation time are allowed to differ from those obtained from fitting to the linear shear data in Figure 2a. The revised values of  $a$  and  $\lambda$  are reported alongside those obtained from shear flow testing in Table 3. The revised values of  $a$  are smaller, 0.63 for 5 g/L and 0.92 for 10 g/L, while the relaxation parameter decreases by over an order of magnitude to give similar values (29 ms for 5 g/L cf., 23 ms for 10 g/L). These results are consistent with those previously reported for a wormlike micellar solution<sup>45</sup> and for different commercial thickeners.<sup>46</sup>

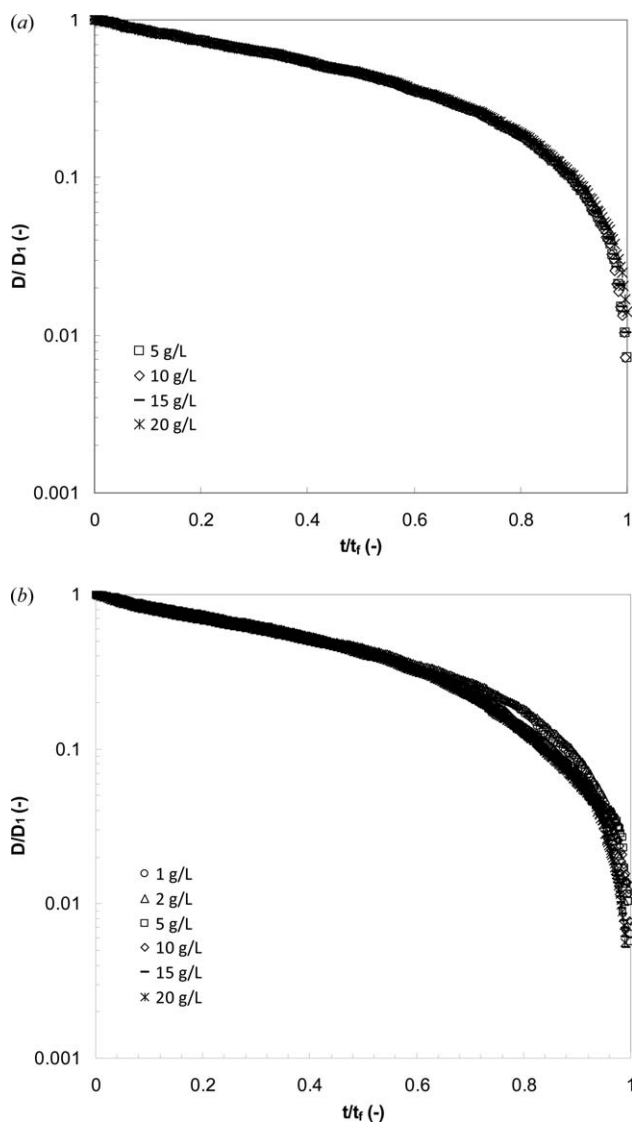


**Figure 7. Time-concentration superposition of the filament stretching data in Figure 5, where time is normalized by the experimental filament rupture time: (a)  $\kappa/\iota$ -hybrid carrageenan gum and (b) guar gum (reproduced from Torres and coworkers<sup>1</sup>).**

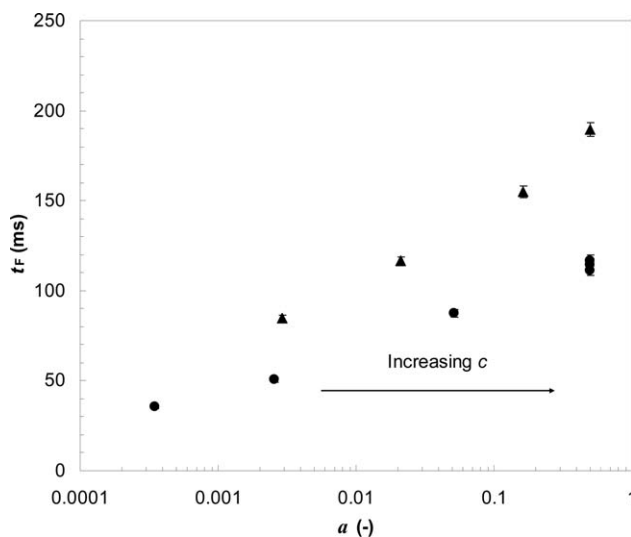


**Figure 8. Relationship between filament rupture time, obtained from extensional testing, and mobility parameter obtained from shear flow data.**

Symbols: circles—guar gum, triangles— $\kappa/\iota$ -hybrid carrageenan gum solutions.

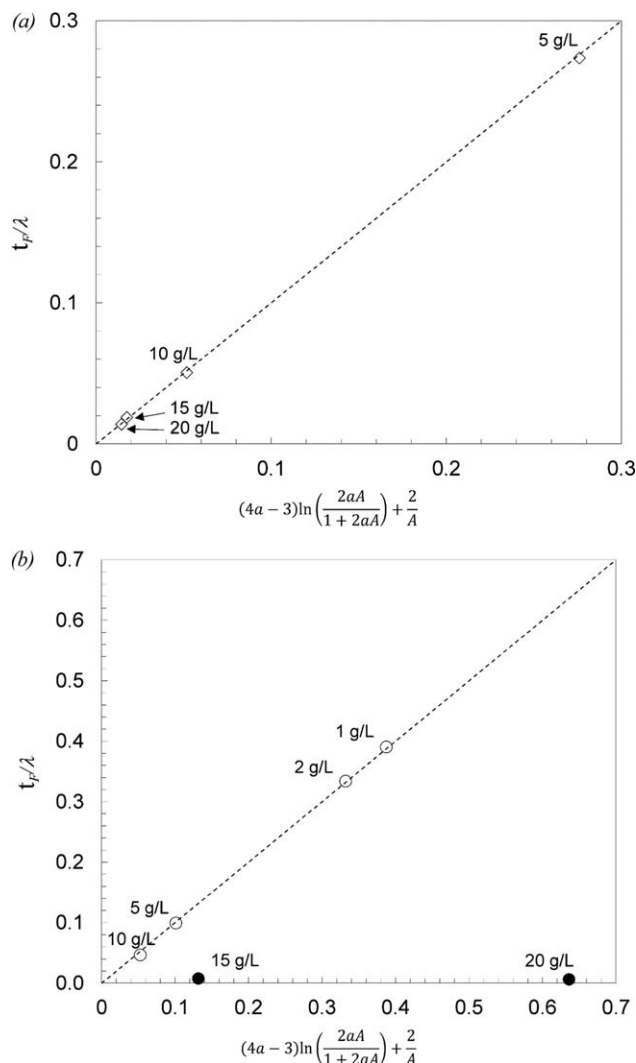


**Figure 9.** Comparison of the left- and right-hand sides of Eq. 25 for (a)  $\kappa/\lambda$ -hybrid carrageenan gum and (b) guar gum solutions.

Open circles—guar gum in semidilute region; solid circles—guar gum in entangled regime; triangles— $\kappa/\lambda$ -hybrid carrageenan. Labels indicate gum concentration.

Comparing the guar gum shear data in Figure 2a with the extensional data in Figure 6, it can be seen that the extensional response becomes substantially independent of solution concentration at  $c > 10$  g/L. In contrast, the shear flow apparent viscosity increases by approximately two orders of magnitude between  $c = 10$  g/L and 20 g/L. These results indicate that different physical mechanisms govern the deformation response and it is unlikely that a simple, single mode, model will cease to describe both behaviors. A multi-mode formulation is likely to be needed for the entangled regime.

#### Time-concentration superposition and rupture time

An alternative means of describing the extensional behavior of guar gum and  $\kappa/\lambda$ -hybrid carrageenan gum solutions, seemingly independently of solution regime, is to use time-concentration superposition as previously reported.<sup>1,2</sup> In this approach, the nondimensional filament diameter is plotted against normalized time, where time is normalized by the filament rupture time. The plots demonstrate that  $\kappa/\lambda$ -hybrid

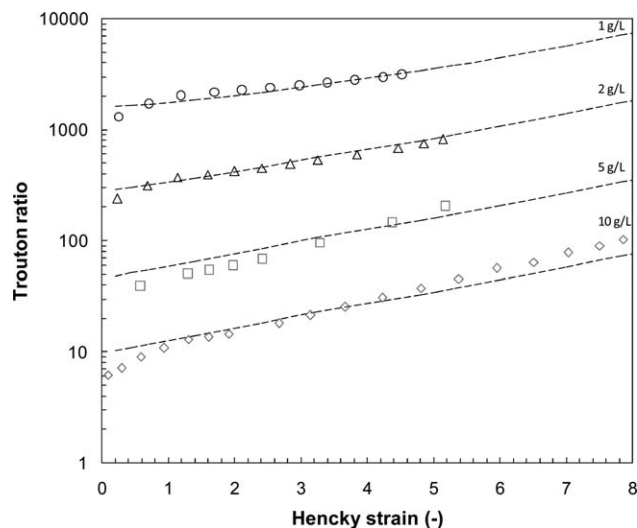


**Figure 10.** Effect of Hencky strain on Trouton ratio, for different guar gum concentrations.

Symbols show experimental data reported by Torres and coworkers.<sup>1</sup> Solid loci represent predictions of the Trouton ratio via Eqs. 4 and 22.

carrageenan gum solutions (Figure 7a) and guar gum solutions in both the semidilute and entangled regime (Figure 7b) collapse onto a single master curve; analogous behavior has been reported for other biopolymeric solutions, such as cellulose,<sup>47</sup> where self-similar filament thinning behavior is observed when the time is normalized by the polymer relaxation time. The parameter in this semiempirical model is the filament rupture time, which increases monotonically with gum concentration and is less sensitive to concentration at higher values:  $t_F$  approaches an asymptote in the entangled regime, in a similar fashion to the mobility parameter (see Figure 3b). Figure 8 shows that the two parameters,  $t_F$  and  $a$ , are closely correlated.

Insight into this behavior can be gained from examining Eq. 20. As the nondimensional filament diameter,  $D/D_1$ , tends to zero, the time,  $t$ , tends to the filament rupture time,  $t_F$ , viz

$$(4a-3)\ln\left(\frac{2aA}{1+2aA}\right) + \frac{2}{A} = \frac{t_F}{\lambda} \quad (25)$$

where

$$A = \frac{\lambda\alpha}{\eta_0 D_1} \quad (26)$$

Close examination of Eq. 25 reveals that the filament rupture time,  $t_F$ , actually decreases with increasing mobility parameter but increases with increasing zero shear rate viscosity. The trend shown in Figure 8 can be explained by the fact that both the mobility parameter and zero shear rate viscosity increase with increasing solution concentration; in this case, the increase in  $t_F$  due to the increasing solution viscosity outweighs the decrease in  $t_F$  due to increasing mobility parameter.

This result suggests that the filament rupture time can be estimated from the shear flow tests. This is tested by evaluating the LHS of Eq. 25, using the parameters listed in Table 1, and comparing the result with the  $t_F$  values divided by the relaxation time. One could also multiply the LHS

by  $\lambda$  to give a comparison of estimated against experimental times. Figure 9 shows that the equality is obeyed for the  $\kappa/\iota$ -hybrid carrageenan gum solutions over the entire concentration range investigated, and the guar gum solutions in the semidilute regime. The predictive relationship does not hold for the guar gum solutions in the entangled regime.

Equation 25 also provides a prediction of filament rupture time if the product  $aA$  is large so that the argument of the log term approaches unity. This gives

$$t_F \approx \frac{2\lambda}{A} = \frac{2\eta_0 D_0}{\alpha} \quad (27)$$

Substitution of this result into Eq. 20 yields

$$(4a-3)\ln\left(\frac{\frac{t_F}{\lambda}\left(\frac{D}{D_1}\right)+4a}{\frac{t_F}{\lambda}+4a}\right) - \frac{t_F}{\lambda}\left(\frac{D}{D_1}\right) = \frac{t_F}{\lambda}\left(\frac{t}{t_F}-1\right) \quad (28)$$

Here, the nondimensional filament diameter appears scaled by the ratio of the filament rupture time to the relaxation time. This scaling gives insight into why time-concentration superposition gives the master curve in Figure 8. It is also instructive to note that the steady-state extensional viscosity for a Giesekus fluid<sup>25</sup> is given by  $\eta_E \approx \frac{2\eta_0}{a}$ , which explains the presence of this grouping in Eqs. 27 and 29.

For the case where  $A$  is large and the mobility parameter  $a = 0.5$  (the upper limit suggested in the literature<sup>43,44</sup>), it can be shown that Eq. 20 predicts a rupture time longer than that given by Eq. 27, namely

$$t_F \approx \frac{3\lambda}{A} = \frac{3\eta_0 D_0}{\alpha} \quad (29)$$

For the guar gum solutions tested in the entangled regime, the condition of  $aA$  being large is not met; hence, Eq. 27 could not be used to predict the filament rupture time. With  $c = 10$  g/L, however, the mobility parameter  $a = 0.5$  and the product  $aA = 28.5$ ; Eq. 29 predicts a rupture time of 125ms which compares reasonably with the experimental value of 111 ms.

### Trouton ratio

The Trouton ratio<sup>48</sup> quantifies the relationship between the shear and extensional viscosities. For a uniaxial extensional flow, the Trouton ratio,  $Tr$ , is given by

$$Tr = \frac{\eta_E(\dot{\epsilon})}{\eta(\sqrt{3}\dot{\epsilon})} \quad (30)$$

where the extensional and shear viscosities,  $\eta_E$  and  $\eta$ , respectively, are evaluated at the Hencky strain rate,  $\dot{\epsilon}$ , and shear rate equivalent to  $\sqrt{3}\dot{\epsilon}$ . The Hencky strain for cylindrical filament thinning can be evaluated from<sup>17</sup>

$$\epsilon = 2\ln\left(\frac{D_0}{D(t)}\right) \quad (31)$$

The  $Tr$  values for the guar gum solutions in the semidilute guar gum regime, evaluated at different Hencky strains, are compared with the Giesekus model predictions (calculated using  $\eta_E$  from Eq. 21 and  $\eta$  from Eq. 4) in Figure 10. The same comparison for  $\kappa/\iota$ -hybrid carrageenan gum is shown in the Appendix, Figure A3.  $Tr$  is always  $>3$ , the value expected for a Newtonian fluid, confirming that studies of the type presented here are required

if these materials are to be simulated reliably. There is broad agreement, over four orders of magnitude, between the experimental values and the model predictions. Good quantitative agreement is again evident with small  $c$ , at the lower end of the semidilute regime, and greater deviation evident at the upper end of the semidilute regime for guar gum solutions. The qualitative trend is captured for both  $c = 5$  g/L and 10 g/L, and the quantitative differences are close enough to give reasonable estimates. There is significant disagreement between the experimental values of  $Tr$  and the model predictions for the entangled regime for guar gum solutions, where  $c = 15$  g/L and 20 g/L. The origin of this disagreement can be seen by examining the differences in the values of the mobility parameter and relaxation time according to whether the fitting was carried out with shear or extensional data; these are given for the upper end of the semidilute regime in Table 3. When making the transition to the entangled regime, the dynamics of the polymer solution are not sufficiently described by one characteristic timescale alone; both reputation dynamics and unentangled chain stretching are contributory factors. The single-mode formulation of the Giesekus fluid used in this work cannot capture both of these contributions, and is, hence, unable to predict the response of the fluid in the entangled regime. Good quantitative agreement was obtained for the  $\kappa/\iota$ -hybrid carrageenan gum solutions (see Appendix, Figure A3). These results provide confidence in using the expressions developed here as a reasonable starting point to describe both the shear and extensional response of these gum solutions, and possibly other biomacromolecular materials, in the semidilute regime.

### Conclusions

A simple expression is presented describing the extensional behavior of a Giesekus fluid undergoing filament stretching. This expression, and one for simple shear reported previously by Giesekus,<sup>5</sup> was used to analyze sets of shear and extensional rheological data reported for aqueous solutions of guar gum<sup>1</sup> and new experimental data obtained for  $\kappa/\iota$ -hybrid carrageenan gum solutions at concentrations ranging from 1–20 g/L. The range of guar gum concentrations studied found to span the transition from the semidilute to entangled regime, based on measurements of the intrinsic viscosity and surface tension.

A single set of Giesekus parameters was found to provide a good quantitative description of both simple and extensional shear behavior for guar gum solutions in the semidilute regime and all the  $\kappa/\iota$ -hybrid carrageenan gum solutions. The parameters were dependent on gum concentration, and the Trouton ratio deviated strongly from the Newtonian value of 3. These findings indicate that the Giesekus model can be used to describe the rheology of these materials in CFD simulations. It also suggests that simple shear tests can be used to give a reliable estimate of their extensional behavior.

At higher guar gum concentrations, both the simple and extensional shear behavior gave poorer fits to the expressions for a single term Giesekus fluid. For solution concentrations toward the upper limit of the semidilute regime ( $c = 5$  and 10 g/L), the expressions still fitted the data well but with separate mobility parameters and relaxation times for simple and extensional shear modes. This could be attributed to the

effect of chain overlap on extension over simple shear. At the highest concentration studied the expressions did not describe the datasets well.

The filament thinning datasets all collapsed to a common curve for that material when presented in terms of the fractional rupture time. The filament-thinning expression derived from the Giesekus model provided insight into this behavior.

## Acknowledgments

The authors acknowledge financial support (POS-A/2012/116) for MDT from Xunta de Galicia's Consellería de Cultura, Educación e Ordenación Universitaria of Spain, and the European Union's European Social Fund. Helpful and insightful comments from the reviewers are also gratefully acknowledged.

## Notation

### Roman letters

$A$  = dimensionless group  
 $a$  = Giesekus mobility parameter  
 $s_1$  = Szyszkowski fitting parameter, N/m  
 $s_2$  = Szyszkowski fitting parameter, g/L  
 $c$  = solution concentration, g L<sup>-1</sup>  
 $D$  = filament diameter, m  
 $D_0$  = initial filament diameter, m  
 $D_1$  = initial filament diameter, m  
 $\mathbf{I}$  = identity tensor  
 $K^*$  = power-law prefactor, various  
 $k$  = Huggins parameter  
 $k_c$  = time constant, s<sup>1-n</sup>  
 $k'$  = proportionality constant, various  
 $N_1$  = first normal stress difference, Pa  
 $N_2$  = second normal stress difference, Pa  
 $n$  = power law exponent  
 $n_2$  = parameter in shear expression  
 $p$  = hydrostatic pressure, Pa  
 $r$  = radial direction, m  
 $Tr$  = Trouton ratio  
 $t$  = time, s  
 $t_F$  = filament rupture time, s  
 $\mathbf{v}$  = velocity vector, m s<sup>-1</sup>  
 $v_r$  = radial velocity, m s<sup>-1</sup>  
 $X$  = shape coefficient

### Greek letters

$\alpha_0$  = solvent surface tension, N m<sup>-1</sup>  
 $\alpha$  = surface tension, N m<sup>-1</sup>  
 $\dot{\epsilon}$  = Hencky strain rate, s<sup>-1</sup>  
 $\epsilon$  = Hencky strain  
 $\dot{\gamma}$  = one-dimensional shear rate, s<sup>-1</sup>  
 $\dot{\gamma}_{rr}$  = radial direction extensional rate, s<sup>-1</sup>  
 $\dot{\gamma}_{zz}$  = axial direction extensional rate, s<sup>-1</sup>  
 $\dot{\gamma}$  = rate-of-strain-tensor, s<sup>-1</sup>  
 $\eta$  = Apparent shear viscosity, Pa s  
 $\eta_{app}$  = apparent viscosity, Cross model, Pa s  
 $\eta_E$  = extensional viscosity, Pa s  
 $\eta_0$  = zero-shear-rate viscosity, Pa s  
 $\eta_{red}$  = reduced viscosity, L g<sup>-1</sup>  
 $\eta_s$  = solvent viscosity, Pa s  
 $[\eta]$  = intrinsic viscosity, L g<sup>-1</sup>  
 $\Lambda$  = group used within shear expression  
 $\lambda$  = relaxation time, s  
 $\sigma$  = total stress tensor, Pa  
 $\sigma_{rr}$  = radial direction total stress, Pa  
 $\sigma_{zz}$  = axial direction total stress, Pa  
 $\tau$  = extra stress tensor, Pa  
 $\tau_{rr}$  = radial direction extensional stress, Pa  
 $\tau_{zz}$  = axial direction extensional stress, Pa

## Literature Cited

- Torres MD, Hallmark B, Wilson DI. Effect of concentration on shear and extensional rheology of guar gum solutions. *Food Hydrocolloids*. 2014;40:85–95.
- Chesterton A, Meza B, Moggridge G, Sadd P, Wilson. Rheological characterisation of cake batters generated by planetary mixing: elastic versus viscous effects. *J Food Eng*. 2011;105(2):332–342.
- Anna SL, McKinley GH. Elasto-capillary thinning and breakup of model elastic liquids. *J Rheol*. 2001;45(1):115.
- Steffe J. *Rheological Methods in Food Process Engineering*. East Lansing: Freeman Press, 1996.
- Giesekus H. A simple constitutive equation for polymer fluids based on the concept of deformation-dependent tensorial mobility. *J Non-Newtonian Fluid Mech*. 1982;11:69–109.
- Chenlo F, Moreira R, Pereira C, Silva C. Rheological modelling of binary and ternary systems of tragacanth, guar gum and methylcellulose in dilute range of concentration at different temperatures. *LWT-Food Sci Technol*. 2009;42:519–524.
- Chenlo F, Moreira R, Silva C. Rheological properties of aqueous dispersions of tragacanth and guar gums at different concentrations. *J Texture Stud*. 2010;41:396–415.
- Bourbon A, Pinheiro A, Ribeiro C. Characterization of galactomannans extracted from seeds of *Gleditsia triacanthos* and *Sophora japonica* through shear and extensional rheology. *Food Hydrocolloids*. 2010;24(2–3):184–192.
- Launay B, Cuvelier G, Martinez-Reyes S. Viscosity of locust bean, guar and xanthan gum solutions in the Newtonian domain. *Carbohydr Polym*. 1997;34:385–395.
- Cross M. Rheology of non-Newtonian fluids: a new flow equation for pseudoplastic systems. *J Colloid Sci*. 1965;20:417–437.
- Hilliou L, Larotonda FDS, Abreu M, Sereno AM, Gonçalves MP. The impact of seaweed life phase and postharvest storage duration on the chemical and rheological properties of hybrid carrageenans isolated from Portuguese *Mastocarpus stellatus*. *Carbohydr Polym*. 2012;87:2655–2663.
- Souza HKS, Hilliou L, Bastos M, Gonçalves MP. Effect of molecular weight and chemical structure on thermal and rheological properties of gelling  $\kappa/\iota$ -hybrid carrageenan solutions. *Carbohydr Polym*. 2011;85:429–438.
- Hilliou L, Larotonda FDS, Abreu M, Ramos AM, Sereno AM, Gonçalves MP. Effect of extraction parameters on the chemical structure and gel properties of  $\kappa/\iota$ -hybrid carrageenans obtained from *Mastocarpus stellatus*. *Biomol Eng*. 2006;23:201–208.
- Azevedo G, Hilliou L, Bernardo G, Sousa-Pinto I, Adams RW, Nilsson M, Villanueva RD. Tailoring kappa/iota-hybrid carrageenan from *Mastocarpus stellatus* with desired gel quality through pre-extraction alkali treatment. *Food Hydrocolloids*. 2013;31:94–102.
- Tatham J, Carrington S, Odell J, Gamboa A, Muller A, Saez A. Extensional behavior of hydroxypropyl guar solutions: optical rheometry in opposed jets and flow through porous media. *J Rheol*. 1995;39:961–986.
- Duxenneuner M, Fischer P, Windhab E, Cooper-White J. Extensional properties of hydroxypropyl ether guar gum solutions. *Biomacromolecules*. 2008;9:2989–2996.
- Vadillo DC, Tuladhar TR, Mulji AC, Jung S, Hoath SD, Mackley MR. Evaluation of the inkjet fluid's performance using the "Cambridge Trimaster" filament stretch and break-up device. *J Rheol*. 2010;54(2):261.
- Li J-M, Burghardt WR, Yang B, Khomami B. Flow birefringence and computational studies of a shear thinning polymer solution in axisymmetric stagnation flow. *J Non-Newtonian Fluid Mech*. 1998;74(1):151–193.
- Quinzani LM, McKinley GH, Brown RA, Armstrong RC. Modeling the rheology of polyisobutylene solutions. *J Rheol*. 1990;34(5):705.
- Holz T, Fischer P, Rehage H. Shear relaxation in the nonlinear-viscoelastic regime of a Giesekus fluid. *J Non-Newtonian Fluid Mech*. 1999;88(1–2):133–148.
- McKinley GH. Using filament stretching rheometry to predict strand formation and processability in adhesives and other non-Newtonian fluids. *J Non-Newtonian Fluid Mech*. 2000;39:321–337.
- Bird RB, Weist JM. Constitutive equations for polymeric liquids. *Annu Rev Fluids Mech*. 1995;27:169–193.
- Bird RB. Anisotropic Effects in Dumbbell Kinetic Theory. *J Rheol*. 1985;29(5):519.



24. Wang Y, Xu J, Bechtel E, K.W. K. Melt shear rheology of carbon nanofiber/polystyrene composites. *Rheologica Acta*. 2006;45:919–941.
25. Bird RB, Armstrong RC, Hassager O. *Dynamics of polymeric liquids. Volume 1 - Fluid Mechanics*, 2nd ed. New York: Wiley, 1987.
26. Nielsen LE. *Polymer Rheology*. New York: Marcel Dekker, 1977.
27. Entov VM, Hinch EJ. Effect of a spectrum of relaxation times on the capillary thinning of a filament of elastic liquid. *J Non-Newtonian Fluid Mech*. 1997;72(1):31–53.
28. Warner HR. Kinetic theory and rheology of dilute suspensions of finitely extendible dumbbells. *Ind Eng Chem Fundam*. 1972;11(3):379–387.
29. Yao M, McKinley GH, Debbaut B. Extensional deformation, stress relaxation and necking failure of viscoelastic filaments. *J Non-Newtonian Fluid Mech*. 1998;79(2–3):469–501.
30. Sachsenheimer D, Hochstein B, Buggisch H, Willenbacher N. Determination of axial forces during capillary breakup of liquid filaments—the tilted CaBER method. *Rheologica Acta*. 2012;51:909–923.
31. Clasen C, Eggers J, Fontelos MA, Li J, McKinley GH. The beads on a string structure of viscoelastic threads. *J Fluid Mech*. 2006;556:283–308.
32. Stelter M, Brenn G, Yarin AL, Singh RP, Durst F. Validation and application of a novel elongational device for polymer solutions. *J Rheology*. 2000;44:595.
33. McKinley GH, Tripathi A. How to extract the Newtonian viscosity from capillary breakup measurements in a filament rheometer. *J Rheol*. 2000;44(3):653.
34. Lindner A, Vermant J, Bonn D. How to obtain the elongational viscosity of dilute polymer solutions? *Phys A*. 2003;319:125–133.
35. Szyszkowski B Von. Experimentelle Studien über kapillare Eigenschaften der wässrigen Lösungen von Fettsäuren. *Z Phys Chem*. 1908;64:385–414.
36. Bouyer E, Mekhloufi G, Rosilio V, Grossiord J-L, Agnely F. Proteins, polysaccharides, and their complexes used as stabilizers for emulsions: alternatives to synthetic surfactants in the pharmaceutical field? *Int J Pharm*. 2012;436(1):359–378.
37. Marangoni A, Narine S. *Physical Properties of Lipids*. New York: Marcel Dekker, 2002.
38. Moreira R, Chenlo F, Silva C, Torres MD, Díaz-Varela D, Hilliou L, Argence H. Surface tension and refractive index of guar and tragacanth gums aqueous dispersions at different polymer concentrations, polymer ratios and temperatures. *Food Hydrocolloids*. 2012;28(2):284–290.
39. Macosko CW. *Rheology: Principles, Measurements and Applications*. New York: Wiley VCH, 1994.
40. Ma X, Pawlik M. Intrinsic viscosities and Huggins constants of guar gum in alkali metal chloride solutions. *Carbohydr Polym*. 2007;70(1):15–24.
41. Azevedo G, Bernardo G, Hilliou L. NaCl and KCl phase diagrams of kappa/iota-hybrid carrageenans extracted from *Mastocarpus stellatus*. *Food Hydrocolloids*. 2014;37:116–123.
42. Dobrynin AV, Colby RH, Rubinstein M. Scaling theory of polyelectrolyte solutions. *Macromolecules*. 1995;28:1859–1871.
43. Schleiniher G. A remark on the Giesekus viscoelastic fluid. *J Rheol*. 1991;35(6):1157.
44. Yoo JY, Choi HC. On the steady simple shear flows of the one-mode Giesekus fluid. *Rheologica Acta*. 1989;28(1):13–24.
45. Yesilata B, Clasen C, McKinley GH. Non linear shear and extensional flow dynamics of a wormlike surfactant solutions. *J Non-Newtonian Fluid Mech*. 2006;133:73–90.
46. Kheirandish S, Guybaidullin I, Willenbacher N. Shear and elongational flow behavior of acrylic thickener solutions. Part II: effect of gel content. *Rheologica Acta*. 2009;48:397.
47. Haward SJ, Sharma V, Butts CP, McKinley GH, Rahatekar SS. Shear and Extensional Rheology of Cellulose/Ionic Liquid Solutions. *Biomacromolecules*. 2012;13:1688–1699.
48. Trouton F. On the coefficient of viscous traction and its relation to that of viscosity. *Proc R Soc London Ser A*. 1906;77(519):426–440.

## Appendix

### Surface tension

The surface tension between the  $\kappa/\iota$ -hybrid carrageenan gum solutions and air at 21°C was determined experimentally using the sessile drop method with a Kruss Drop Shape Analyser 100 device. Values reported are the mean from at least 10 measurements. The influence of  $\kappa/\iota$ -hybrid carrageenan gum concentration was satisfactorily fitted to the Szyszkowski equation<sup>35</sup>

$$\frac{\alpha}{\alpha_0} = 1 - s_1 \ln \left( 1 + \frac{c}{s_2} \right) \quad (\text{A1})$$

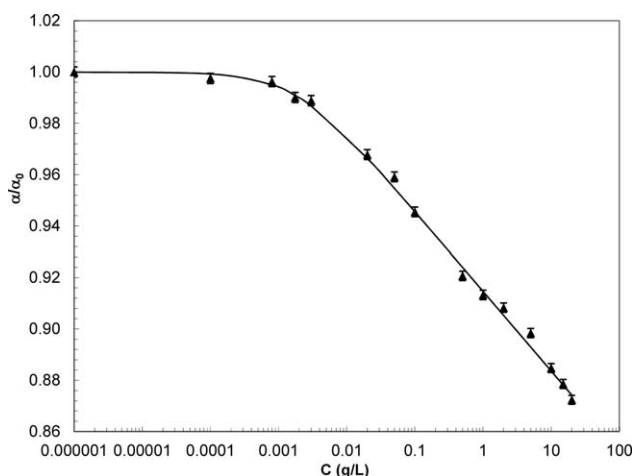


**Figure A1.** Effect of  $\kappa/\iota$ -hybrid carrageenan gum concentration on surface tension relative to water.

Solid trend line shows Eq. A.1 fitted to the  $\kappa/\iota$ -hybrid carrageenan gum data with parameters  $s_1 = 0.0135$  and  $s_2 = 0.0018$  g/L.

where  $\alpha_0$  is the surface tension of the solvent,  $c$  the concentration of the surfactant and  $s_1$  and  $s_2$  are fitting parameters. This fit is shown in Figure A1.

**Table A1. Parameter Values Obtained for Cross-Williamson Model, Eq. A2, for Aqueous  $\kappa/\iota$ -hybrid Carrageenan Gum Solutions Prepared at Different Concentration<sup>a</sup>**

$c$ (g/L)	$\eta_0$ (Pa s)	$k_c$ (s <sup>1-n</sup> )	$n$ (-)	$R^2$	$s$ (Pa s)
5	0.041 ± 0.02 <sup>d</sup>	0.066 ± 0.002 <sup>d</sup>	0.37 ± 0.01 <sup>b</sup>	0.996	0.0015
10	0.41 ± 0.03 <sup>c</sup>	0.45 ± 0.02 <sup>c</sup>	0.38 ± 0.01 <sup>a,b</sup>	0.995	0.0018
15	4.2 ± 0.2 <sup>b</sup>	1.7 ± 0.1 <sup>b</sup>	0.39 ± 0.01 <sup>a</sup>	0.990	0.0023
20	15.1 ± 0.3 <sup>a</sup>	2.4 ± 0.1 <sup>a</sup>	0.41 ± 0.01 <sup>a,b</sup>	0.991	0.0021

<sup>a</sup>Data are presented as mean ± standard deviation.

Data values in a column with different superscript letters are significantly different at the  $P \leq 0.05$  level.

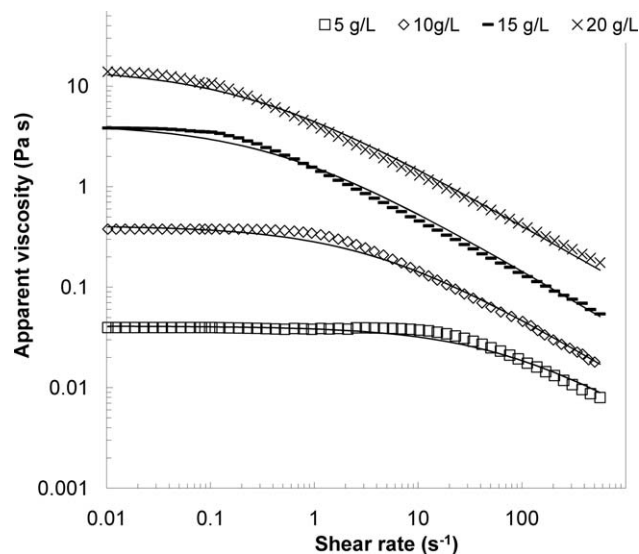


**Figure A2.** Flow curves of representative aqueous  $\kappa/\lambda$ -hybrid carrageenan gum solutions prepared at different concentrations.

Symbols: 5 g/L (squares); 10 g/L (diamonds); 15 g/L (dashes); and 20 g/L (crosses). Dashed loci indicate model fit obtained using Cross model, Eq. A.2, parameters in Table A1.

### Cross model

The experimental flow curves for  $\kappa/\lambda$ -hybrid carrageenan gum samples were satisfactorily fitted ( $R^2 > 0.990$ , standard error  $< 0.0023$  Pa s) to the Cross-Williamson model, Eq. A2

$$\frac{\eta_{app}}{\eta_0} = \frac{1}{1 + k_c \dot{\gamma}^{(1-n)}} \quad (A2)$$

where  $\eta_0$  is the zero-shear rate viscosity,  $k_c$  is the time constant

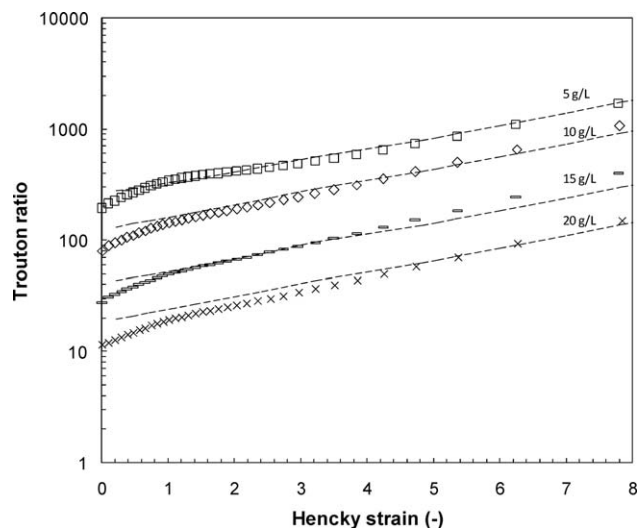


**Figure A3.** Effect of Hencky strain on Trouton ratio, for different  $\kappa/\lambda$ -hybrid carrageenan gum concentrations.

Symbols: 5 g/L (squares); 10 g/L (diamonds); 15 g/L (dashes); and 20 g/L (crosses). Solid loci represent predictions of the Trouton ratio via Eqs. 4 and 21.

and  $n$  is the flow index. Parameters for the fit to the Cross-Williamson model are given in Table A1, and the fit is shown in Figure A2.

### Trouton ratio

The effect of Hencky strain on the Trouton ratio for different  $\kappa/\lambda$ -hybrid carrageenan gum concentrations is shown in Figure A3.

Manuscript received Apr. 8, 2014, and revision received Aug. 14, 2014.